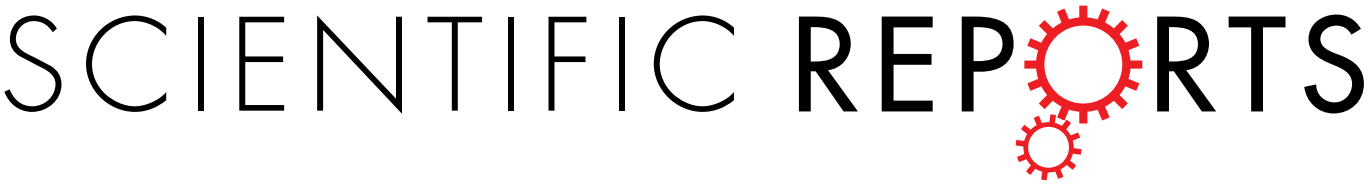

OPEN

Characteristics of multiple Fano resonances in waveguide-coupled surface plasmon resonance sensors based on waveguide theory

Received: 12 September 2017
Accepted: 26 January 2018
Published online: 07 February 2018

Liu Yang[1], Jicheng Wang[1,2], Li-zhi Yang[1], Zheng-Da Hu[1], Xiaojun Wu[3] & Gaige Zheng[4]

We observe and analyze multiple Fano resonances and the plasmon-induced transparency (PIT) arising from waveguidecoupled surface plasmon resonance in a metal-dielectric Kretschmann configuration. It is shown that the simulation results for designed structures agree well with those of the dispersion relation of waveguide theory. We demonstrate that the coupling between the surface plasmon polariton mode and multi-order planar waveguide modes leads to multiple Fano resonances and PIT. The obtained results show that the number of Fano resonances and the linewidth of resonances depend on two structural parameters, the *Parylene C* and SiO_2 layers, respectively. For the sensing action of Fano resonance, the figure of merit for the sensitivity by intensity is estimated to be 44 times higher than that of conventional surface plasmon resonance sensors. Our research reveals the potential advantage of sensors with high sensitivity based on coupling between the SPP mode and multi-order PWG modes.

The interaction of freely oscillating electrons on a metallic surface with photons can induce surface plasmon polaritons (SPPs). These are electromagnetic waves that propagate along the surface of a metal-insulator interface[1] and exponential evanescent field that is excited by transverse magnetic polarized light perpendicular to the interface. Transverse magnetic polarized light on a prism at an angle greater than the critical angle can generally lead to total internal reflection (TIR) at the interface of the metal and prism in a Kretschmann configuration, and evanescent waves for TIR can match with the wave vector of SPP mode to motivate SPPs. Due to the characteristics of SPPs, optical sensors and biomolecular interactions[1–4] based on SPPs have been investigated widely. However, the metal layer of the conventional prism-based sensors causes a broad surface plasmon resonance (SPR), which can limit the sensitivity and resolution of sensors. More attention is being focused on obtaining a narrower linewidth of resonances to improve their performance in many SPR structures. SPR sensors based on long-range SPPs[5–7] and waveguide (WG)-coupled SPR[2,3,8] have been proposed. WG-coupled SPR sensors combining planar waveguides (PWGs) with SPR can achieve sharp resonance curves for both the p- and s-polarized incident light from the excitation of PWG modes[2,3,9].

Hayashi *et al.* recently achieved coupling between SPPs and PWG modes[10–14]. They proposed a planar multilayer structure that exhibits plasmon-induced transparency (PIT) and Fano resonance in a Kretschmann configuration. PIT is called electromagnetically-induced transparency (EIT)[15,16], because plasmonic effects have an EIT-like lineshape[17] characterized by a sharp transmission band in the middle of a broad absorption band. The interference between a continuum state and a discrete level can cause Fano resonance (FR) with an asymmetric lineshape[18,19], then the coupling between a broad and a narrow resonance can arise from so-called Fano resonance. In the past decade, people have tried to achieve EIT-like and Fano lineshapes in various nanostructures, including plasmonic nanostructures[18–30] and metamaterials[17,31–35]. Hayashi *et al.* demonstrated experimentally and numerically the coupling between a SPP mode and a PWG mode, the reflectivity spectra, and the widths of

[1]School of Science, Jiangsu Provincial Research Center of Light Industrial Optoelectronic Engineering and Technology, Jiangnan University, Wuxi, 214122, China. [2]State Key Laboratory of Millimeter Waves, Southeast University, Nanjing, 210096, China. [3]School of IoT Engineering, Jiangnan University, 214122, Wuxi, China. [4]Jiangsu Key Laboratory for Optoelectronic Detection of Atmosphere and Ocean, School of Physics and Optoelectronic Engineering, Nanjing University of Information Science and Technology, Nanjing, 210044, China. Liu Yang and Jicheng Wang contributed equally to this work. Correspondence and requests for materials should be addressed to J.W. (email: jcwang@jiangnan.edu.cn)

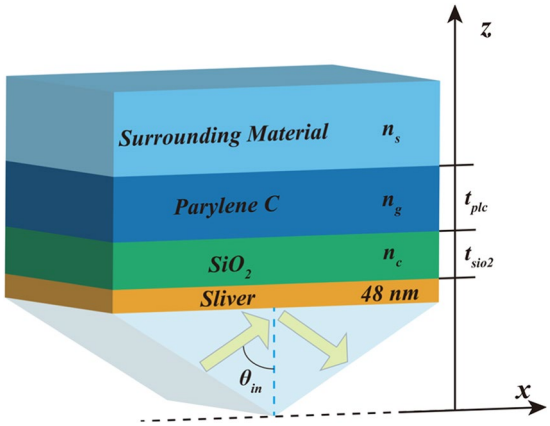

Figure 1. Schematic of metal-dielectric multilayer Kretschmann configuration under TM-polarized light. The refractive index of the prism is assumed as 1.7. SiO_2, *Parylene C*, and the surrounding dielectric layer are placed on Ag film in sequence, and their refractive indices are fixed at $n_c = 1.458$, $n_g = 1.62$, and $n_s = 1.333$, respectively. The thicknesses of the SiO_2, *Parylene C* layers are defined as t_{SiO_2} and t_{plc}, respectively.

FR and PIT lineshapes[10,11]. They also showed an almost perfect analogy between an electromagnetic (EM) system and a system of coupled oscillators (COs)[14]. Although they referred to high-order modes[11], our research provides a detailed explanation.

In this paper, we propose a planar structure of waveguide-coupled SPR sensor, it is a metal-dielectric Kretschmann structure that can achieve multiple Fano resonances and PIT. From the analysis of electromagnetic calculations made for this structure, we illustrate that multiple Fano resonances and PIT are attributed to the coupling between the SPP mode and multi-order PWG modes. The simulation results for a designed structure agree well with those of the dispersion relation of waveguide theory. Also, we demonstrate that two structural parameters respectively govern the number of Fano resonances and the linewidth of resonances. We estimate that the figure of merit of refractive index sensing for the sensitivity by intensity is 44 times higher than that of conventional SPR sensors[14].

Results

We propose a metal-dielectric multilayer Kretschmann configuration under TM-polarized light. This consists of a prism, Ag film, a SiO_2 layer, a *Parylene C* layer, and a surrounding dielectric layer, as shown in Fig. 1. The SiO_2 and surrounding dielectric layer are separated by a *Parylene C* layer whose refractive index is larger than those of the SiO_2 and the surrounding dielectric layers. The three dielectric layers make up a waveguide and the *Parylene C* layer can support PWG modes. We know that a structure consisting of only a semi-infinite dielectric layer adjacent to a metal layer can support SPP mode in a conventional SPR sensor. Therefore, not only SPP mode and PWG modes can be supported, but the coupling of the SPP mode and PWG modes can be achieved if the structural parameters are selected appropriately[10]. In the calculation, the dielectric function of metal is defined by the Drude model as

$$\varepsilon_{Ag}(\omega) = \varepsilon_\infty - \frac{\omega_p^2}{\omega^2 + i\gamma\omega}, \tag{1}$$

where ε_∞ is the infinite frequency dielectric constant, ω_p is the bulk plasma frequency, ω is the angular frequency, and γ is the collision frequency which is related to the dissipation loss in the metal. These parameters are set as 6.0, 1.5×10^{16} rad/s, and 7.73×10^{13} rad/s, respectively[36].

Figure 2(a) shows the map of reflection spectra calculated at different angles under TM-polarized light with a wavelength of 632.8 μm where t_{plc} is assumed to 1.3 μm and t_{SiO_2} is changed from 0 to 1 μm. Figure 2(b,c and d) show the distributions of the magnetic field and field intensity curves corresponding to the three points defined as A, B, and C, respectively. The magnetic field of A is not only concentrated within the *Parylene C* layer and there is one field node throughout the whole map of reflection spectra, but also is focused on the $Ag - SiO_2$ interface, as shown in Fig. 2(b). It is expected that the SPP mode at the interface of Ag film and SiO_2 layer can achieve partial coupling with PWG modes supported in *Parylene C* layer, which can lead to a Fano resonance. Figure 2(c) shows that the magnetic field is strong at the interface of Ag film and the SiO_2 layer, which indicates excitation of the SPP mode (corresponding to B). Figure 2(d) shows that the strong and almost complete coupling between the SPP mode and PWG modes can be observed in the *Parylene C* layer, which can also lead to a sharp Fano resonance. From the distributions of the magnetic field, if the Fano resonance is far from the broad SPP resonance (corresponding to C), the magnetic field on the $Ag - SiO_2$ interface is weaker, indicating that the degree of coupling between the SPP mode and PWG modes is strong. Conversely, if the Fano resonance is close to the broad SPP resonance (corresponding to A), the magnetic field on the $Ag - SiO_2$ interface is stronger, indicating that the degree of the coupling between SPP mode and PWG modes is weak. Here, we can conclude that the distributions of the magnetic field can reflect the degree of coupling between the SPP mode and PWG modes.

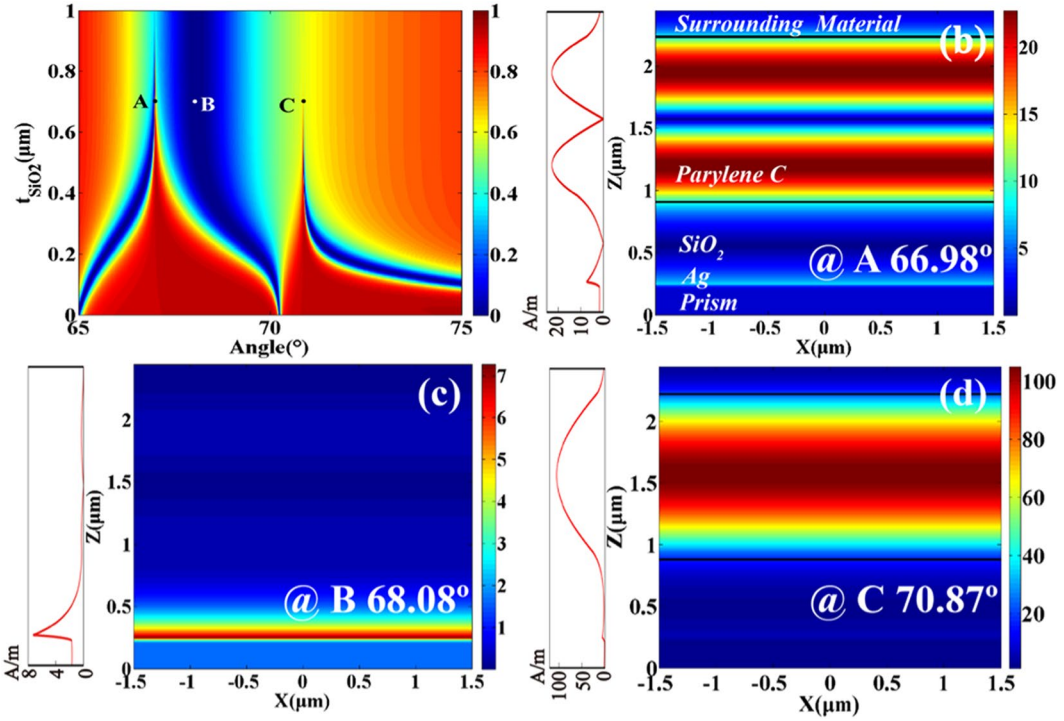

Figure 2. The thickness of *Parylene C* layer $t_{plc} = 1.3\ \mu m$, $n_c = 1.458$, $n_g = 1.62$, $n_s = 1.333$. (**a**) Contour plots of the reflection versus incident angle and the thickness of the SiO_2 layer. (**b**–**d**) Distributions of the magnetic field and field intensity curves are plotted at the three points (the three points are under different angles and $t_{SiO_2} = 0.7\ \mu m$), as shown in Fig. 2(a). The division of the structure area is shown in Fig. 2(b), and the material between two black lines is *Parylene C* layer.

When t_{SiO_2} is fixed at 0.7 μm, the reflectivity calculated under TM polarization light with a wavelength of 632.8 μm for the proposed structure shows that the Fano resonances have a shift and the number of Fano resonances increases with the change of $_{tplc}$ from 1.1 μm to 1.8 μm, as shown in Fig. 3, while for $t_{plc} = 1.5\ \mu m$, a typical line-shape of PIT appears. The distributions of the magnetic field and field intensity curves of these points marked in Fig. 3 are shown in Fig. 4. When t_{plc} is fixed at 1.1 μm, two Fano resonances, I and II, correspond to the magnetic field distributions I-first order and II-zero order, respectively, in Fig. 4. Similarly, the three Fano resonances III, IV, and V with $t_{plc} = 1.4\ \mu m$ correspond to the magnetic field distributions III-second order, IV-first order, and V-zero order, and four Fano resonances VI, VII, VIII, and IX with $t_{plc} = 1.7\ \mu m$ correspond to the magnetic field distributions VI-third order, VII-second order, VIII-first order, and IX-zero order, respectively. It is clear that the magnetic field distributions of zero-order Fano resonances are concentrated within the PWG layer and have no field node, which is attributed to the complete coupling of the SPP mode and TM_0 PWG modes. For the magnetic field distributions of first-, second-, and third-order Fano resonances, the magnetic fields exist in the $Ag - SiO_2$ interface and PWG layer with one, two and three field nodes, respectively, which respectively depend on the partial coupling between the SPP mode and the TM_1, TM_2, and TM_3 PWG modes. Therefore, the positions of Fano resonances move with an increase in the number of Fano resonances. We can also conclude that the distributions of the magnetic field are used to observe the coupling between the SPP mode and different-order PWG modes. Note that we do not show all simulated Fano resonances in reflectivity curves. We can use a part of the simulated Fano resonances to explicitly illustrate that multiple Fano resonances are attributed to the coupling between the SPP mode and multi-order PWG modes.

We turn to theory to further clarify why the number of Fano resonances increases and Fano resonances shift with the increase of t_{plc}. According to the dispersion relation of waveguides[37], the plots of the generalized guide index b versus the generalized frequency V for TM modes with parameters of the designed structure are depicted in Fig. 5. We can also obtain the cutoff V and cutoff thickness of the waveguide h in a designed structure corresponding to each mode, as shown in Table 1. Although Hayashi *et al.* refer to high-order modes[11] refer to high-order modes, they provide no explanation for their appearance. We will theoretically analyze the reasons for the appearance of high-order PWG modes.

In Fig. 5 and Table 1, the generalized frequency V is called as the cutoff V when the generalized guide index b is equal to zero. It is also obvious that a kind of TM_m ($m = 0, 1, 2, 3 \cdots$) PWG mode can be supported by a waveguide if the generalized frequency V is equal to or larger than the cutoff V (or the waveguide h is equal to or larger than the cutoff h). Therefore, from Fig. 5 and Table 1, we can surmise that the waveguide in the proposed structure can support multi-order PWG modes with t_{plc} ranging from 1.1 to 1.8 μm. Under the appropriate structural parameters, the SPP mode can couple with different orders of PWG modes, which leads to multiple Fano resonances. In a fixed range, the number of Fano resonances increases, while the positions of Fano resonances move

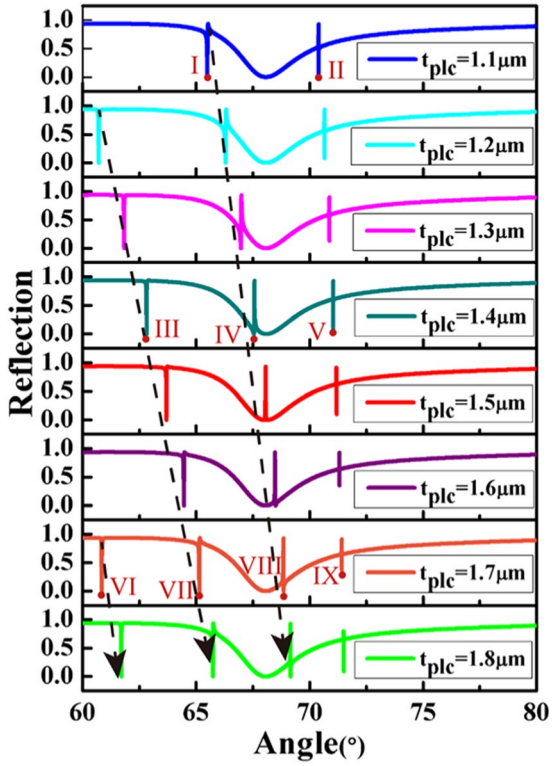

Figure 3. Reflection curves plotted as a function of incident angle with t_{plc} ranging from 1.1 to 1.8 μm. The dashed lines indicate the position shift of multiple Fano resonances. The thickness of SiO_2 layer $t_{SiO_2} = 0.7\ \mu m$, $n_c = 1.458$, $n_g = 1.62$, $n_s = 1.333$.

with it. For example, when $t_{plc} = 1.1\ \mu m$ in simulation, there are four Fano resonances, as shown in Fig. 6, which suggests that the SPP mode couples with four orders of PWG modes. In theory, the thickness of the *Parylene C* t_{plc} is approximately equal to the cutoff thickness 1.1043 μm from Table 1, so four orders of PWG modes can be supported in a waveguide layer, and the coupling between the SPP mode and four orders of PWG modes can lead to four Fano resonances. It is clear that the simulation results for the designed structure agree well with those of the dispersion relation of waveguide theory.

From Fig. 3, we can see that a typical lineshape of PIT appears with $t_{plc} = 1.5\ \mu m$. Therefore, we discuss the effect of the thickness of SiO_2 on the lineshape of PIT, when t_{plc} is 1.5 μm. Figure 7 shows the reflection spectra with different thicknesses of SiO_2 under TM polarization light with a wavelength of 632.8 μm. It is clear that the linewidth of PIT is increasingly narrow as the thickness of SiO_2 increases. Also, the linewidth of Fano resonance on the right side of the PIT shows a similar change, and the amplitude of Fano resonance can be affected by the thickness of SiO_2.

The shift of TM_0 Fano resonance curves, which can be considered the sensitivity for sensors, is caused by a change in the refractive index (RI) of surrounding material.It is shown in Fig. 8. To compare with the performance of the conventional SPR sensors, we usually use either an angular shift of the $\Delta\theta_{res}$ curve (sensing by angular modulation) or a change in the reflectance ΔR at a fixed angle (sensing by intensity modulation) to describe the change in the resonance curve caused by a change in the RI Δn[4,38]. The sensitivity by intensity is given by

$$S_I(\theta) = \lim_{\Delta n \to 0} \frac{\Delta R}{\Delta n} = \frac{\partial R(\theta)}{\partial n}. \tag{2}$$

It is convenient to compare the sensitivities of different types of sensors by using the figure of merit for sensitivity by intensity, given by

$$FOM_I = \max_{\theta} |S_I(\theta)|, \tag{3}$$

which is the maximum value of the sensitivity by intensity. For a conventional SPR sensor, it consists of a 50 nm-thick Au film deposited on a SF10 prism, the SPP resonance in the conventional SPR sensor is broad and has a small slope. Therefore, Δn as small as 1×10^{-2} is required to produce a change in the reflectance of $\Delta R_{\max} = 0.35$ the ratio $\Delta R_{\max}/\Delta n = 35 \mathrm{RIU}^{-1}$[14]. However, the present TM_0 Fano sensor can produce the change $\Delta R_{\max} = 0.15402$ (the maximum value in the Fig. 8, when Δn is as small as 1×10^{-4}. The ratio $\Delta R_{\max}/\Delta n$ is 1540.2 RIU^{-1}. These values suggest that the present Fano sensor has an extremely high sensitivity

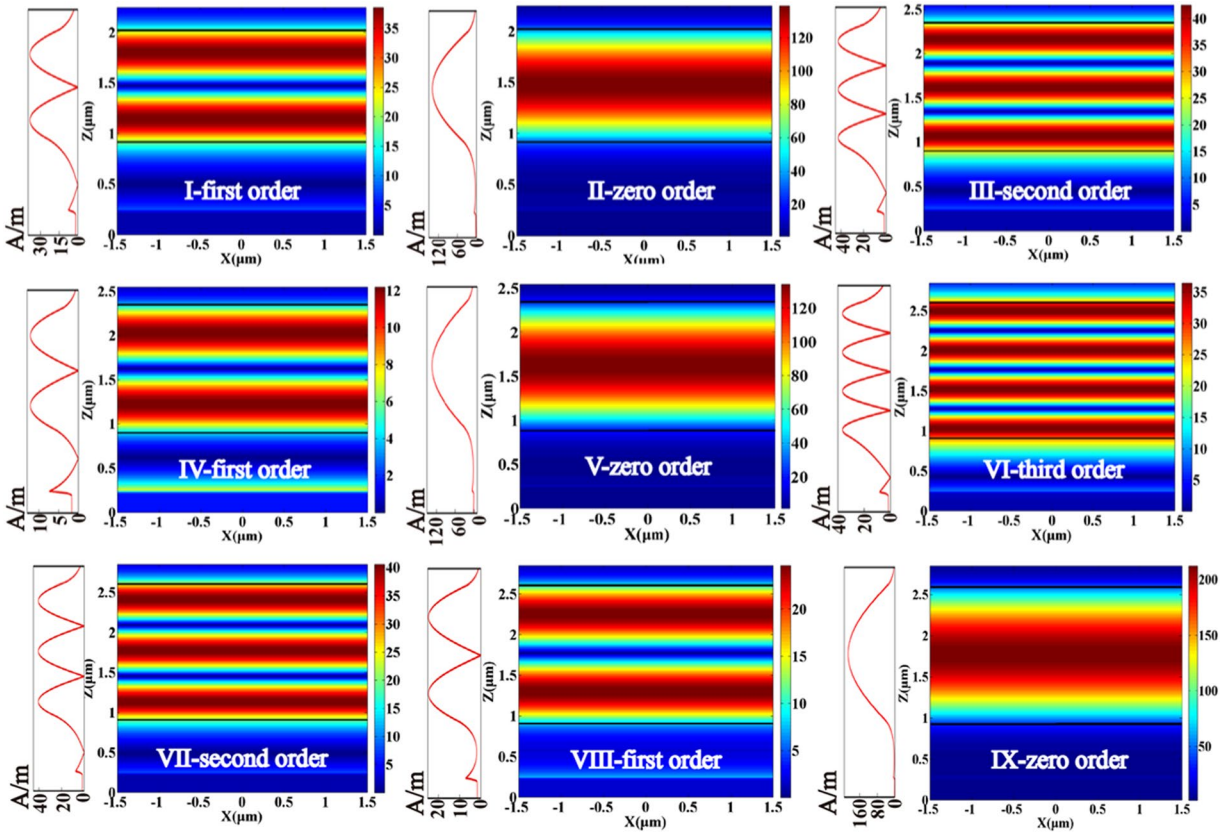

Figure 4. Distributions of the magnetic field and field intensity curves are plotted to present the variation tendency of SPP mode and different-order PWG modes at these points as shown in Fig. 3. The other parameters used are the same as those in Fig. 3. The material between two black lines is *Parylene C* layer.

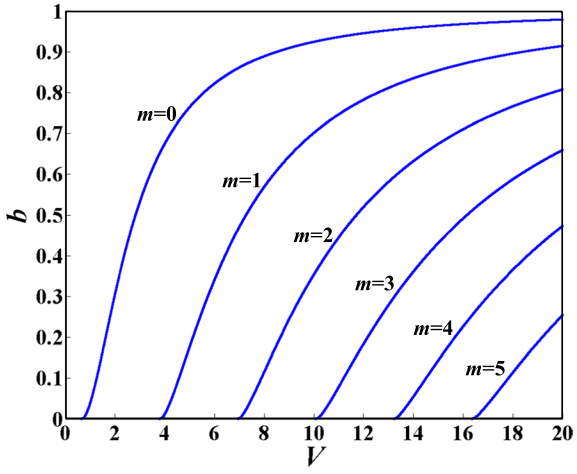

Figure 5. Plots of b versus V for TM modes with a wavelength of 632.8 μm calculated by equation 21. The parameters used in equation 21 are $n_g = 1.62$, $n_s = 1.333$, $n_c = 1.458$.

by intensity compared to that of the conventional SPR sensor. It is estimated that FOM_I of the present TM_0 Fano sensor is at least 44 times than that of the conventional SPR sensor.

Discussion

In conclusion, we propose a metal-dielectric multilayer Kretschmann structure that can achieve multiple Fano resonances and PIT resulting from the coupling between the SPP mode and multi-order PWG modes. We conclude that the coupling between the SPP mode and multi-order PWG modes can lead to multiple Fano resonances from electromagnetic calculations. It is important that the calculations of the dispersion relation of waveguide

Guide mode	Cutoff V	Cutoff thickness h (μm)
$m = 0$	$V = 0.6699$	$h = 0.073287$
$m = 1$	$V = 3.8115$	$h = 0.41697$
$m = 2$	$V = 6.9531$	$h = 0.76066$
$m = 3$	$V = 10.095$	$h = 1.1043$
$m = 4$	$V = 13.236$	$h = 1.448$
$m = 5$	$V = 16.378$	$h = 1.7917$

Table 1. Cutoff V and cutoff thickness h corresponding to each mode. The parameters used in equations 22–23 are the same as those in Fig. 5.

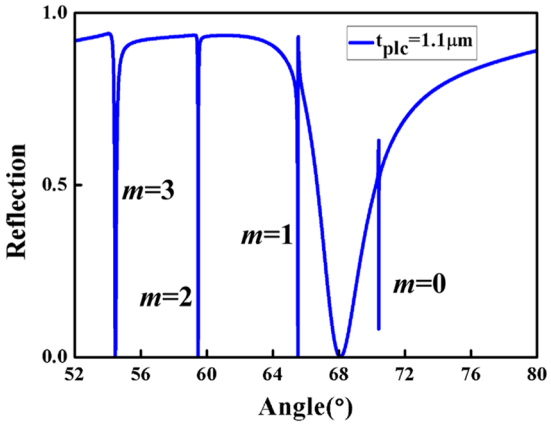

Figure 6. Reflection curve is plotted as a function of incident angle. The thickness of the *Parylene C* layer is $t_{plc} = 1.1\ \mu m$, the thickness of the SiO_2 layer is $t_{SiO_2} = 0.7\ \mu m$, $n_c = 1.458$, $n_g = 1.62$, $n_s = 1.333$.

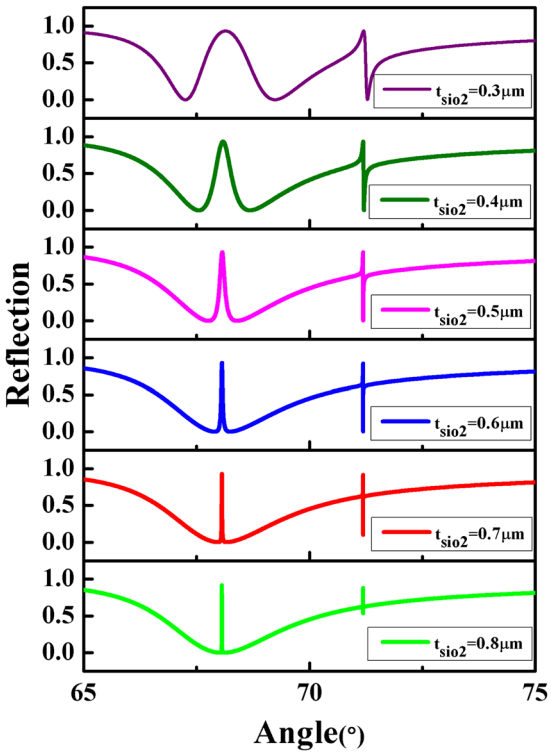

Figure 7. Reflection curves are plotted as a function of incident angle with t_{SiO_2} ranging from 0.3 to 0.8 μm. The thickness of the *Parylene C* layer is $t_{plc} = 1.5\ \mu m$, $n_c = 1.458$, $n_g = 1.62$, $n_s = 1.333$.

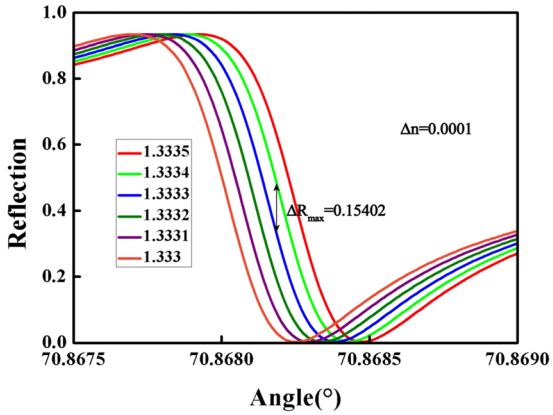

Figure 8. Shift of TM_0 Fano resonance for the structure with $t_{SiO_2} = 0.7\ \mu m$ and $t_{plc} = 1.3\ \mu m$. The refractive index of surrounding material changes from 1.333 to 1.3335 with steps of $\Delta n = 0.0001$. $n_c = 1.458$, $n_g = 1.62$.

theory are consistent with those of the designed structure. Also, we observe that two structural parameters, the thicknesses of SiO_2 and *Parylene C*, influence the number of Fano resonances and the linewidth of resonances, respectively. We also analyze the sensing action of the proposed TM_0 Fano resonance. Its the figure of merit for the sensitivity by intensity is 44 times greater than that of a conventional SPR sensor. Our results may pave the way in the coupling between the SPP mode and multi-order PWG modes and for the design of efficient sensors with high sensitivity.

Methods

A TM mode has a magnetic field component, h_y and two electric field components, e_x and e_z. The transverse electric field component e_x is normal to the waveguide surface and the direction of propagation. In addition, the two electric field components can be expressed in terms of h_y. Specifically, we obtain[37]

$$e_x(x) = \frac{\beta}{\omega\varepsilon_0 n^2} h_y(x) \tag{4}$$

$$e_z(x) = -j\frac{1}{\omega\varepsilon_0 n^2}\frac{dh_y(x)}{dx}. \tag{5}$$

The boundary conditions for h_y, e_z, and e_x are met if h_y and $(1/n^2)/(dh_y/dx)$ are continuous at the boundaries. We write h_y in the cover, film and substrate regions as

$$h_y(x) = H_c e^{-\gamma_c x} \tag{6}$$

$$h_y(x) = H_f \cos\left(k_f x + \varphi'\right) \tag{7}$$

$$h_y(x) = H_s e^{\gamma_s (x+h)}, \tag{8}$$

where H_c, H_f, H_s, and φ' are constants to be determined. By matching the boundary values, we obtain the dispersion relation or characteristic equation for TM modes:

$$k_f h = \tan^{-1}\frac{n_f^2}{n_c^2}\frac{\gamma_c}{k_f} + \tan^{-1}\frac{n_f^2}{n_s^2}\frac{\gamma_s}{k_f} + m\pi, \tag{9}$$

where

$$k_f = \sqrt{k^2 n_f^2 - \beta^2} \tag{10}$$

$$\gamma_s = \sqrt{\beta^2 - k^2 n_s^2} \tag{11}$$

$$\gamma_c = \sqrt{\beta^2 - k^2 n_c^2}. \tag{12}$$

The mode number m is an integer. When β and three of the four constants are determined, the TM problem is solved. The fourth constant, say H_f or H_c, represents the amplitude of the TM mode. In particular, H_c is the magnetic field intensity at the cover-film boundary and H_f is the peak magnetic field intensity of the TM mode

in question. To circumvent the difficulties in the calculation process, Kogelnik and Ramaswany introduced generalized parameters[39].

Several generalized parameters[39–41] can describe TM modes guided by three-layer step-index waveguides. These generalized parameters are

(a) the asymmetry measure,

$$a = \frac{n_s^2 - n_c^2}{n_f^2 - n_s^2} \tag{13}$$

(b) the generalized frequency, also known as the generalized film thickness,

$$V = kh\sqrt{n_f^2 - n_s^2} \tag{14}$$

(c) the generalize guide index,

$$b = \frac{N^2 - n_s^2}{n_f^2 - n_s^2} \tag{15}$$

The generalized parameters a and b are the differences $n_s^2 - n_c^2$ and $N^2 - n_s^2$ normalized with respect to $n_f^2 - n_s^2$. In other words, these generalized parameters are in terms of the differences of squared indices rather than the indices themselves.

Some manipulation will show that

$$k_f h = kh\sqrt{n_f^2 - N^2} = V\sqrt{1 - b} \tag{16}$$

$$\gamma_s h = kh\sqrt{N^2 - n_s^2} = V\sqrt{b}, \tag{17}$$

and

$$\gamma_c h = kh\sqrt{N^2 - n_c^2} = V\sqrt{a + b}. \tag{18}$$

The extra parameter can be either

$$c = \frac{n_s^2}{n_f^2} \tag{19}$$

or

$$d = \frac{n_c^2}{n_f^2} = c - a(1 - c). \tag{20}$$

Using these expressions in equation 9, we can obtain the dispersion relation for TM modes. In terms of generalized parameters, we have

$$V\sqrt{1 - b} = \tan^{-1}\frac{1}{d}\sqrt{\frac{a + b}{1 - b}} + \tan^{-1}\frac{1}{c}\sqrt{\frac{b}{1 - b}} + m\pi. \tag{21}$$

For a given waveguide operating at a specific wavelength, the values of nf, n_s, n_c, h, and λ are known. The values of a, c, d, and V can be calculated from the waveguide parameters. For each set of a, V and c, we determine b numerically from equation 21 for TM modes. There may be one or more solutions for b, depending on V, a, and c. Each solution for b corresponds to a guided mode. The largest value of b corresponds to $m = 0$.

As noted earlier, each solution of b corresponds to a guided mode. As the film thickness decreases, corresponding to a smaller V, b becomes smaller. As b of a given mode approaches zero, the mode approaches its cutoff. As noted previously, the cutoff condition is $b = 0$. By setting b to zero, we obtain, from equation 21 that the cutoff V for the TM_m mode is

$$V = m\pi + \tan^{-1}\left(\frac{\sqrt{a}}{d}\right) = m\pi + \tan^{-1}\left(\frac{n_f^2}{n_c^2}\sqrt{a}\right). \tag{22}$$

In other words, a TM_m mode is supported by a thin-film waveguide if the film thickness is at least

$$h = \frac{m\pi + \tan^{-1}\left(\frac{n_f^2}{n_c^2}\sqrt{a}\right)}{2\pi\sqrt{n_f^2 - n_s^2}}\lambda. \tag{23}$$

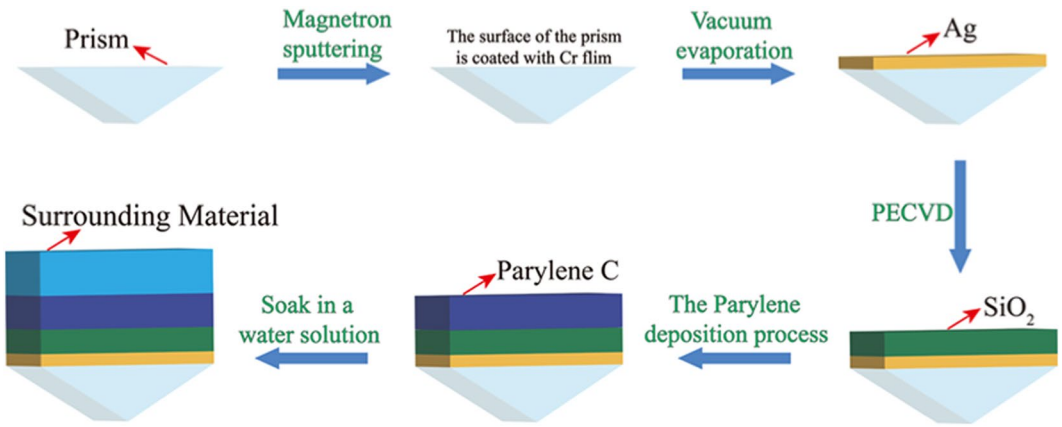

Figure 9. Process flow diagram of the proposed device fabrication.

Fabrication process of the proposed structure. Figure 9 shows a design scheme of the fabrication process for the proposed structure. First, the surface of the prism is coated with 5 nm of Cr film to plate a metal film using the magnetron sputtering method, which is one of physical vapor deposition (PVD). Next, the Ag layer is deposited with an electron-beam evaporator system. The SiO_2 is then deposited using the plasma enhanced chemical vapor deposition (PECVD) method. *Parylene C* can then be deposited by the *Parylene* deposition process. Finally, the whole structure is soaked in a water solution that is a sensing medium.

Numerical simulation. Rigorous couple wave analysis (RCWA) method simulations are performed to obtain the contour plots of the reflection, magnetic field distributions, and reflection spectra. All simulated figures are drawn using MATLAB software after processing the data, including plots of the generalized guide index *b* versus the generalized frequency *V* for TM modes, according to the dispersion relation of waveguides.

References

1. Raether, H. Surface plasmons on smooth and rough surfaces and on gratings. *Springer Tracks in Modern Physics* **111**, 4–39 (1988).
2. Knoll, W. Interfaces and thin films as seen by bound electromagnetic waves. *Annual Review of Physical Chemistry* **49**, 569–638 (1998).
3. Homola, J. Surface plasmon resonance sensors for detection of chemical and biological species. *Chemical reviews* **108**, 462–493 (2008).
4. Homola, J., Yee, S. S. & Gauglitz, G. Surface plasmon resonance sensors. *Sensors and Actuators B:Chemical* **54**, 3–15 (1999).
5. Dostalek, J., Kasry, A. & Knoll, W. Long range surface plasmons for observation of biomolecular binding events at metallic surfaces. *Plasmonics* **2**, 97–106 (2007).
6. Berini, P. Long-range surface plasmon polaritons. *Advances in optics and photonics* **1**, 484–588 (2009).
7. Nenninger, G. G., Tobiska, P., Homola, J. & Yee, S. S. Long-range surface plasmons for high-resolution surface plasmon resonance sensors. *Sensors and Actuators B: Chemical* **74**, 145–151 (2001).
8. Chien, F. C. & Chen, S. J. A sensitivity comparison of optical biosensors based on four different surface plasmon resonance modes. *Biosensors and bioelectronics* **20**, 633–642 (2004).
9. Salamon, Z., Macleod, H. A. & Tollin, G. Coupled plasmon-waveguide resonators: a new spectroscopic tool for probing proteolipid film structure and properties. *Biophysical journal* **73**, 2791–2797 (1997).
10. Hayashi, S., Nesterenko, D. V. & Sekkat, Z. Fano resonance and plasmon-induced transparency in waveguide-coupled surface plasmon resonance sensors. *Applied Physics Express* **8**, 022201 (2015).
11. Hayashi, S., Nesterenko, D. V., Rahmouni, A. & Sekkat, Z. Observation of Fano line shapes arising from coupling between surface plasmon polariton and waveguide modes. *Applied Physics Letters* **108**, 051101 (2016).
12. Sekkat, Z. *et al*. Plasmonic coupled modes in metal-dielectric multilayer structures: Fano resonance and giant field enhancement. *Optics express* **24**, 20080–20088 (2016).
13. Nesterenko, D. V., Hayashi, S. & Sekkat, Z. Extremely narrow resonances, giant sensitivity and field enhancement in low-loss waveguide sensors. *Journal of Optics* **18**, 065004 (2016).
14. Hayashi, S., Nesterenko, D. V. & Sekkat, Z. Waveguide-coupled surface plasmon resonance sensor structures: Fano lineshape engineering for ultrahigh-resolution sensing. *Journal of Physics D: Applied Physics* **48**, 325303 (2015).
15. Harris, S. E. Electromagnetically induced transparency. *Physics Today* **50**, 36 (1997).
16. Fleischhauer, M., Imamoglu, A. & Marangos, J. P. Electromagnetically induced transparency: Optics in coherent media. *Reviews of modern physics* **77**, 633 (2005).
17. Zhang, S., Genov, D. A., Wang, Y., Liu, M. & Zhang, X. Plasmon-induced transparency in metamaterials. *Physical Review Letters* **101**, 07401 (2008).
18. Luk'yanchuk, B. *et al*. The fano resonance in plasmonic nanostructures and metamaterials. *Nature materials* **9**, 707 (2010).
19. Wang, J., Sun, L., Hu, Z. D., Liang, X. & Liu, C. C. Plasmonic-induced transparency of unsymmetrical grooves shaped metal-insulator-metal waveguide. *AIP Advances* **4**, 123006 (2014).
20. Zentgraf, T., Zhang, S., Oulton, R. F. & Zhang, X. Ultranarrow coupling-induced transparency bands in hybrid plasmonic systems. *Physical Review B* **80**, 195415 (2009).
21. Liu, N. *et al*. Plasmonic analogue of electromagnetically induced transparency at the drude damping limit. *Nature materials* **8**, 758 (2009).
22. Taubert, R., Hentschel, M., Kastel, J. & Giessen, H. Classical analog of electromagnetically induced absorption in plasmonics. *Nano letters* **12**, 1367–1371 (2012).
23. Ishikawa, A., Oulton, R. F., Zentgraf, T. & Zhang, X. Slow-light dispersion by transparent waveguide plasmon polaritons. *Physical Review B* **85**, 155108 (2012).
24. Christ, A. *et al*. Controlling the fano interference in a plasmonic lattice. *Physical Review B* **76**, 201405 (2007).

25. Sonnefraud, Y. *et al*. Experimental realization of subradiant, superradiant, and fano resonances in ring/disk plasmonic nanocavities. *ACS nano* **4**, 1664–1670 (2010).
26. Lassiter, J. B. *et al*. Designing and deconstructing the fano lineshape in plasmonic nanoclusters. *Nano letters* **12**, 1058–1062 (2012).
27. Gallinet, B. & Martin, O. J. Influence of electromagnetic interactions on the line shape of plasmonic fano resonances. *ACS nano* **5**, 8999–9008 (2011).
28. Francescato, Y., Giannini, V. & Maier, S. A. Plasmonic systems unveiled by fano resonances. *ACS nano* **6**, 1830–1838 (2012).
29. Forestiere, C., Dal Negro, L. & Miano, G. Theory of coupled plasmon modes and fano-like resonances in subwavelength metal structures. *Physical Review B* **88**, 155411 (2013).
30. Verellen, N. *et al*. Mode paritycontrolled fano- and lorentz-like line shapes arising in plasmonic nanorods. *Nano Letters* **14**, 2322–2329 (2014).
31. Papasimakis, N., Fedotov, V. A., Zheludev, N. I. & Prosvirnin, S. L. Metamaterial analog of electromagnetically induced transparency. *Physical Review Letters* **101**, 253903 (2008).
32. Ooi, K., Okada, T. & Tanaka, K. Mimicking electromagnetically induced transparency by spoof surface plasmons. *Physical Review B* **84**, 115405 (2011).
33. Gu, J. *et al*. Active control of electromagnetically induced transparency analogue in terahertz metamaterials. *Nature communications* **3**, 1151 (2012).
34. Tassin, P. *et al*. Electromagnetically induced transparency and absorption in metamaterials: the radiating two-oscillator model and its experimental confirmation. *Physical review letters* **109**, 187401 (2012).
35. Osley, E. J. *et al*. Fano resonance resulting from a tunable interaction between molecular vibrational modes and a double continuum of a plasmonic metamolecule. *Physical review letters* **110**, 087402 (2013).
36. Zheng, G., Zou, X., Chen, Y., Xu, L. & Rao, W. Fano resonance in graphene-mos 2 heterostructure-based surface plasmon resonance biosensor and its potential applications. *Optical Materials* **66**, 171–178 (2017).
37. Chen, C. L. Foundations for guided-wave optics. *John Wiley and Sons Inc* (2006).
38. Nesterenko, D. V. & Sekkat, Z. Resolution estimation of the au, ag, cu, and al single-and double-layer surface plasmon sensors in the ultraviolet, visible, and infrared regions. *Plasmonics* **8**, 1585–1595 (2013).
39. Kogelnik, H. & Ramaswamy, V. Scaling rules for thin-film optical waveguides. *Applied Optics* **13**, 1857–1862 (1974).
40. Kogelnik, H. Theory of dielectric waveguides. *Integrated optics* **8**, 13–81 (1975).
41. Bennett, G. A. & Chen, C. L. Wavelength dispersion of optical waveguides. *Applied Optics* **19**, 1990–1995 (1980).

Acknowledgements

This work is supported by the National Natural Science Foundation of China (Grant Nos 11504139, 11504140), the Natural Science Foundation of Jiangsu Province (Grant Nos BK20140167, BK20140128), the China Postdoctoral Science Foundation (2017M611693), and the Open Fund of State Key Laboratory of Millimeter Waves (Grant No. K201802).

Author Contributions

J.W., X.W. and G.Z. conceived the idea. L.Y. and L.Z.Y. developed the model. L.Y. and L.Z.Y. carried out the numerical simulation. L.Y. and J.W. wrote the manuscript and plotted the figures. X.W., J.W. and Z.D.H. supervised the project. All authors discussed the results and commented on the manuscript.

Additional Information

Competing Interests: The authors declare no competing interests.

Publisher's note: Springer Nature remains neutral with regard to jurisdictional claims in published maps and institutional affiliations.